SCIENCE CHINA Materials

ARTICLES

mater.scichina.com link.springer.com

Published online 8 May 2017 | 10.1007/s40843-017-9035-8
Sci China Mater 2017, 60(11): 1121–1128

Atomic-scale Pt clusters decorated on porous α-$Ni(OH)_2$ nanowires as highly efficient electrocatalyst for hydrogen evolution reaction

Hongchao Yang[1,2], Changhong Wang[1,2], Feng Hu[2], Yejun Zhang[2], Huan Lu[2] and Qiangbin Wang[1,2,3*]

ABSTRACT **The synthesis of atomic-scale metal catalysts is a promising but very challenging project. In this work, we successfully fabricated a hybrid catalyst of $Pt_c/Ni(OH)_2$ with atomic-scale Pt clusters uniformly decorated on porous $Ni(OH)_2$ nanowires (NWs) *via* a facile room-temperature synthesis strategy. The as-obtained $Pt_c/Ni(OH)_2$ catalyst exhibits highly efficient hydrogen evolution reaction (HER) performance under basic conditions. In 0.1 mol L^{-1} KOH, the $Pt_c/Ni(OH)_2$ has an onset overpotential of ~0 mV *vs.* RHE, and a significantly low overpotential of 32 mV at a current density of 10 mA cm^{-2}, lower than that of the commercial 20% Pt/C (58 mV). The mass current density data illustrated that the $Pt_c/Ni(OH)_2$ reached a high current density of 6.34 A mg_{Pt}^{-1} at an overpotential of 50 mV, which was approximately 28 times higher than that of the commercial Pt/C (0.223 A mg_{Pt}^{-1}) at the same overpotential, proving the high-efficiency electrocatalytic activity of the as-obtained $Pt_c/Ni(OH)_2$ for HER under alkaline conditions.**

Keywords: atomic-scale, platinum, $Ni(OH)_2$, clusters, hydrogen evolution reaction

INTRODUCTION

Molecular hydrogen is regarded as one of the most efficient, environmentally friendly and renewable energy carriers in the 21st century owing to its unique advantages including high efficiency and natural abundance along with environmental benignity [1,2]. Alkaline water electrolysis is a most economical and sustainable method to produce hydrogen due to unlimited reactant availability, good manufacturing safety, stable output and high product purity [3–6]. Nevertheless, cathodic hydrogen evolution reaction (HER) of alkaline water splitting often suffers from sluggish kinetics, making it critical to develop electrocatalysts with high efficiency to promote the process of HER. Up to now, the platinum–based catalyst is still the best HER electrocatalyst under alkaline conditions due to the low onset overpotential, small Tafel slope and strong durability [7]. Although many non-noble-metal electrocatalysts such as Ni-based alloys [8–12] and Co-based nanocomposites [13–15] have motivated intense research on electrocatalytic HER, their poorer HER performance than Pt-based catalysts enormously restricts their practical applications. Consequently, how to enhance the HER activity of Pt-based materials in basic media is a greatly valuable but very challenging project.

Atomic-scale metal catalysts often show fairly large atom efficiency and high-efficiency catalytic activity, which have attracted widespread attention [16–19]. Decreasing the size of catalysts can increase the specific surface area, which will greatly augment the active sites. Atomic metal catalysts promise higher atom utility in the catalyst and have emerged as a new research frontier [20]. Therefore, designing atomic-scale Pt based hybrid catalysts for HER could greatly improve their electrocatalytic performance.

In addition, another feasible way to enhance the HER activity of Pt in basic media is combination of Pt with 3d-M (M= Mn, Fe, Co, Ni) metal hydroxides, because the edges of the $M(OH)_X$ sites can facilitate dissociation of water and production of hydrogen intermediates, which would adsorb on the nearby Pt surfaces (called absorbed hydrogen, H_a), and subsequently the H_a would combine to generate

[1] School of Nano Technology and Nano Bionics, University of Science and Technology of China, Suzhou 215123, China.
[2] Key Laboratory of Nano-Bio Interface, Division of Nanobiomedicine and i-Lab, Suzhou Institute of Nano-Tech and Nano-Bionics, Chinese Academy of Sciences, Suzhou 215123, China.
[3] College of Materials Sciences and Opto-Electronic Technology, University of Chinese Academy of Sciences, Beijing 100049, China.
* Corresponding author (email: qbwang2008@sinano.ac.cn)

molecular hydrogen [2–23]. Yin *et al.* [21] reported a facile wet-chemical method to realize Pt NWs grown on β-$Ni(OH)_2$ nanosheets, showing a higher HER performance than Pt/C. Meanwhile, α-$Ni(OH)_2$ usually displays superior electrochemical performance to other phases of $Ni(OH)_2$ due to its special intrinsic structure. Gao *et al.* [24] experimentally demonstrated that α-$Ni(OH)_2$ has better OER catalytic activity than β-$Ni(OH)_2$. And we predict that α-$Ni(OH)_2$ can also exhibit more prominent HER performance because α-$Ni(OH)_2$ is isostructural with the hydroxide-rich basic salts of nickel [25]. In α-$Ni(OH)_2$, the anions are loosely intercalated between the hydrated nickel hydroxide sheets, $[Ni(OH)_{2-x}(H_2O)_x]^{x+}$, which would be more likely promoting dissociation of water in alkaline solutions. Consequently, rational design of atomic-scale Pt decorated on α-$Ni(OH)_2$ can provide a large number of active sites and promote dissociation of water to improve the HER performance of the catalyst owing to synergetic chemical coupling effect between Pt and α-$Ni(OH)_2$. However, to the best of our knowledge, there are no any related studies about simultaneously utilizing this synergetic effect on HER electrocatalysts in basic solution.

Herein, we reported a facile synthetic strategy to fabricate a hybrid electrocatalyst of atomic-scale Pt clusters decorated on porous α-$Ni(OH)_2$ NWs ($Pt_c/Ni(OH)_2$). The $Pt_c/Ni(OH)_2$ was synthesized by using weak reductant (NaH_2PO_2) to reduce adsorbed H_2PtCl_6 of the as-obtained porous $Ni(OH)_2$ NWs, and the Pt mass loading was up to 4 wt.%. The $Pt_c/Ni(OH)_2$ catalyst exhibits highly efficient HER performance under basic conditions. The polarization curves demonstrate that the $Pt_c/Ni(OH)_2$ has an onset overpotential of ~0 mV *vs.* RHE, and a significantly low overpotential of 32 mV at a current density of 10 mA cm^{-2}, lower than that of the commercial 20% Pt/C (58 mV) and Pt NPs/$Ni(OH)_2$ (60 mV) at the same current density. The mass current density illustrates that the $Pt_c/Ni(OH)_2$ reaches a high current density of 6.34 A mg_{Pt}^{-1} at an overpotential of 50 mV in 0.1 mol L^{-1} KOH solution, which is approximately 28 and 6.8 times that of commercial Pt/C (0.223 A mg_{Pt}^{-1}) and Pt NPs/$Ni(OH)_2$ (0.922 A mg_{Pt}^{-1}) at the same overpotential, respectively.

EXPERIMENTAL SECTION

Chemicals

All of the materials were purchased and used without further purification. Nickel sulfate hexahydrate ($NiSO_4{\cdot}6H_2O$, AR, ≥98.5%) and sodium hydroxide (NaOH, AR, ≥98%) were purchased from Sinopharm Chemical Reagent Co., Ltd. Sulfuric acid (H_2SO_4, AR, 98%) was purchased from Enox Co., Ltd. Sodium hypophosphite (NaH_2PO_2, AR 99.0%) was purchased from Aladdin Chemistry Co., Ltd. Chloroplatinate acid hexahydrate ($H_2PtCl_6{\cdot}6H_2O$, assay: ≥37.5% Pt basis), potassium hydroxide solution (KOH, HPLC, 45 wt.%) and Pt/C (20 wt.% Pt on Vulcan XC-72R) were purchased from Alfa Aesar. Nafion perfluorinated resin (5 wt.%) solution was purchased from Sigma-Aldrich. Sodium borohydride ($NaBH_4$, >99%) was obtained from Acros Organics.

Synthesis of porous $Ni(OH)_2$ nanowires

In a typical reaction, 5.257 g $NiSO_4{\cdot}6H_2O$ (~20 mmol) and 0.800 g NaOH (~20 mmol) were dissolved in deionized water (40 mL), respectively. After continuous stirring for 30 min, the NaOH solution was slowly added into the $NiSO_4{\cdot}6H_2O$ aqueous solution. Then, the mixture was transferred to a 100-mL Teflon-lined stainless steel autoclave, sealed and aged at 120°C for 24 h in an electric oven. When the reaction was finished and cooled down to room temperature, a large amount of water was added and the as-obtained products were collected by centrifugation. Subsequently, the products were suspended in 200 mL deionized water to form a homogeneous dispersion ($c[Ni(OH)_2]$ = 4 mg mL^{-1}).

Synthesis of atomic-scale $Pt/Ni(OH)_2$

Five mililiter of $Ni(OH)_2$ solution above was added in 10 mL deionized water under stirring condition. Then, 0.1 mL H_2PtCl_6 aqueous (0.1 mol L^{-1}) was added under stirring for 1 h. Afterwards, it was mixed with NaH_2PO_2/H_2O solution and reacted at room temperature for approximately 5 days. And then a light yellow solution was obtained. Subsequently, the as-obtained products were washed with deionized water for several times. The products were suspended in 20 mL deionized water to form a homogeneous dispersion ($c[Ni(OH)_2]$ = 1 mg mL^{-1}).

Synthesis of Pt NPs/$Ni(OH)_2$

Five mililiter of $Ni(OH)_2$ solution was added in 10 mL deionized water under stirring condition. Then, 11.3 μL H_2PtCl_6 aqueous (0.1 mol L^{-1}) was added under stirring for 1 h. Subsequently, it was mixed with $NaBH_4/H_2O$ solution and reacted at room temperature for approximately 30 s. And then a black dispersion liquid was obtained. The as-obtained black products were washed with deionized water for several times.

Characterizations

The morphologies of the products were examined through

a Tecnai G2 F20 S-Twin transmission electron microscope (TEM) at an accelerating voltage of 200 kV, and a Quanta 400 FEG scanning electron microscope (SEM) at 20 kV, respectively. Energy-dispersive spectroscopy (EDS) measurements and high resolution TEM (HRTEM) were also recorded on Tecnai G2 F20 S-TEM. Powder X-ray diffraction (XRD) patterns were recorded on a Bruker D8 Advance powder X-ray diffractometer at a scanning rate of 4° min^{-1}, using Cu-Kα radiation (λ=1.54056 Å). X-ray photoelectron spectroscopy (XPS) data were performed by a PHI 5000 Versaprobe X-ray photoelectron spectrometer, using nonmonochromatized Al-Kα X-ray as the excitation source. Inductively coupled plasma mass spectrometry (ICP-MS) analysis was recorded on a Thermo Fisher Scientific ICAP Qc.

Electrochemical measurement

One milligram of $Pt_c/Ni(OH)_2$ product, 2 mg of Ketjen black (the mass of Pt/C catalyst is 3 mg) and 50 μL of 5 wt.% Nafion solution were dispersed in 0.968 mL of 3:1 (*v*/*v*) water/ethanol by sonication for at least 30 min to form a homogeneous ink. Then 4 μL of the catalyst ink (containing 0.16 μg of Pt catalyst) was loaded onto a glassy carbon electrode of 3 mm in diameter. The HER tests were carried out in a conventional three electrode electrochemical cell by using CHI660E. Linear scanning voltammetry (LSV) was carried out at a scan rate of 50 mV s^{-1} with the pretreated glassy carbon electrode as the working electrode, an Ag/AgCl electrode as the reference electrode and a carbon rod electrode as the counter electrode. All the potentials reported in this work are with iR correction, which are given *vs*. reversible hydrogen electrode (RHE) according to $E_{vs.\ RHE} = E_{vs.\ Ag/AgCl} + E^{\theta}_{Ag/AgCl} + 0.059$ pH.

RESULTS AND DISCUSSION

The atomic-scale Pt clusters decorated on porous α-$Ni(OH)_2$ NWs was prepared *via* a very facile method. First, the porous α-$Ni(OH)_2$ NWs were synthesized according to previous work [19]. $NiSO_4$ solution mixed with NaOH solution was firstly heated at 120°C for 24 h and a light green gelatinous precipitate was obtained. Then H_2PtCl_6/H_2O was added in the $Ni(OH)_2/H_2O$ dispersion under continuous stirring. Subsequently, the above solution was mixed with NaH_2PO_2/H_2O solution and reacted at room temperature for several days to transform into a light yellow solution.

The SEM and TEM image of $Ni(OH)_2$ in Figs S1 and S2 illustrate the morphology of the as-prepared $Ni(OH)_2$ NWs along with a large quantity of porous structures. Then, the powder XRD proves that the sample is α-phase $Ni(OH)_2$ (Fig. S3) [26]. After decorated with atomic-scale Pt, the TEM images in Fig. 1a, b show that the morphology of the as-synthesized $Pt_c/Ni(OH)_2$ was completely inherited from the α-phase $Ni(OH)_2$ without any obvious change (also descripted in SEM image in Fig. S4). The HRTEM image of the $Pt_c/Ni(OH)_2$ in Fig. 1c exhibits obvious lattice fringe of α-$Ni(OH)_2$, but hard to identify the Pt due to its small size and inconspicuous contrast in the HRTEM image. To testify the exist of Pt on the $Ni(OH)_2$ NWs, the high-resolution high-angle annular dark-field (HAADF) STEM image was taken. As shown in Fig. 1d and e, a lot of bright spots were homogeneously dispersed on the $Ni(OH)_2$ NWs with their sizes smaller than 1 nm, illustrating the successful growth of Pt clusters on the $Ni(OH)_2$ NWs. Further, the EDS elemental mapping of the $Pt_c/Ni(OH)_2$ in Fig. 1f demonstrates that the Ni, O and Pt elements are homogeneously distributed in the $Pt_c/Ni(OH)_2$ NWs, suggesting that the atomic-scale Pt clusters are successfully loaded on $Ni(OH)_2$ NWs (for more EDS analyses, see Figs S5 and S6. Another peak of Cu element in the EDS originated from the carbon-coated copper grid substrate and the S element is from the reactant of Na_2SO_4 during the preparation of α-$Ni(OH)_2$ NWs). We surmised that the formation of the $Pt_c/Ni(OH)_2$ was attributed to the porous structure of the $Ni(OH)_2$ NWs, which could adsorb the Pt(IV) ion and provide a reaction field. Following the addition of weak reductant (NaH_2PO_2), the Pt(IV) was slowly reduced to form the atomic-scale Pt clusters. The powder XRD patterns of both $Ni(OH)_2$ and $Pt_c/Ni(OH)_2$ in Fig. 2a show that after the process of loading Pt, the crystalline structure of $Ni(OH)_2$ has not transformed. And there is no obvious diffraction peaks of Pt in the pattern of $Pt_c/Ni(OH)_2$ on account of their small size and low mass loading of Pt.

To detect the surface composition of the catalysts, XPS was measured. In Fig. 2b, the XPS survey spectrum shows the presence of Pt, Ni, and O. The high resolution XPS spectrum of Ni 2p region in Fig. 2c displays two peaks in Ni $2p_{3/2}$ region at 855.8 and 861.4 eV, Ni $2p_{1/2}$ region at 873.7 and 879.4 eV. The peaks at 855.8 and 861.4 eV are assigned to the binding energies for oxidized Ni species and the satellite of the Ni $2p_{3/2}$ peak. And the peaks at 873.7 and 879.4 eV belong to oxidized Ni species and the satellite of the Ni $2p_{1/2}$ peak. After deconvolution of Pt 4f region in Fig. 2d, the peaks at around 71.9 and 74.9 eV are attributed

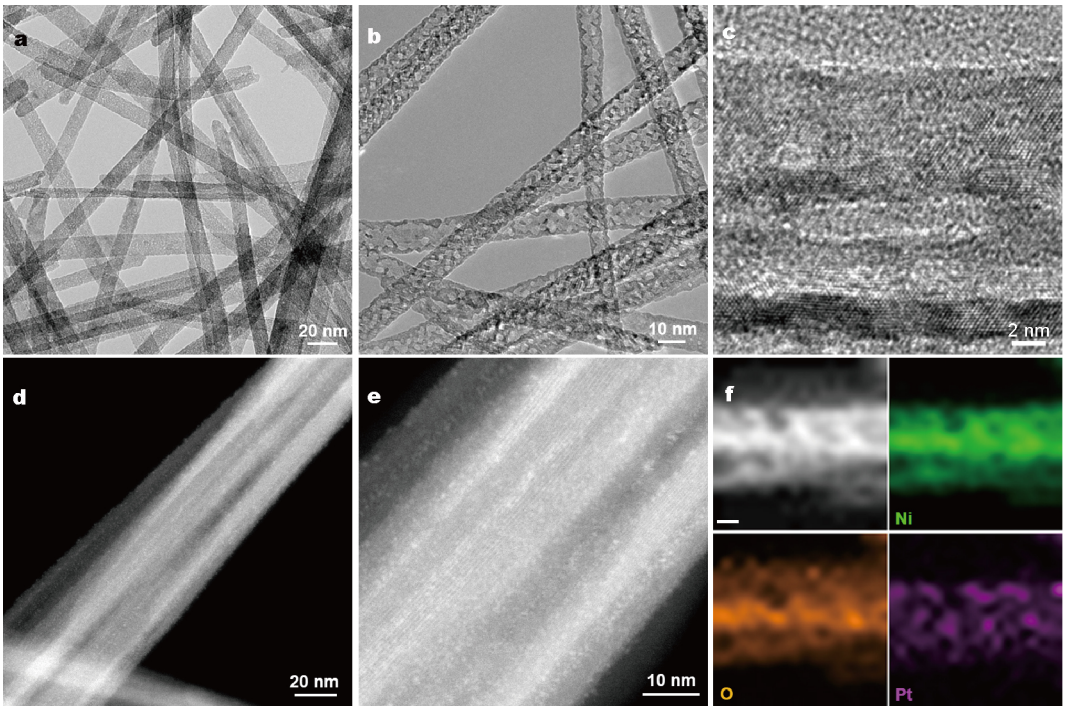

Figure 1 (a, b) TEM images of atomic-scale Pt decorated on porous $Ni(OH)_2$ NWs at different magnifications. (c) HRTEM image of $Pt_c/Ni(OH)_2$ NWs. (d, e) HR-HAADF STEM image of the as-prepared $Pt_c/Ni(OH)_2$. (f) The STEM-EDS elemental mapping of the $Pt_c/Ni(OH)_2$. Scale bars = 20 nm. The HR-HAADF STEM image and elemental mapping of the $Pt_c/Ni(OH)_2$ were measured at a bunch of wires.

to Pt^0, and the peaks at about 72.8 and 76.0 eV are assigned to Pt^{2+}. Integral data reveal that Pt^0 atoms are dominant (59%, red curves in Fig. 2d) and the rest of 41% are Pt^{2+} ions (blue curves in Fig. 2d), respectively. Another peak coexisted in Pt 4f region is Ni 3p peak, which can be ascribed to Ni^{2+} species in $Ni(OH)_2$ (cyan curve in Fig. 2d). Moreover, the survey spectrum and high resolution Ni 2p regions of both $Pt_c/Ni(OH)_2$ and $Ni(OH)_2$ NWs alone in Fig. S7 illustrate that there are no obvious changes in chemical state of Ni(II) after decorating atomic-scale Pt clusters on $Ni(OH)_2$ NWs. The mass loading of Pt on $Pt_c/Ni(OH)_2$ was measured to be about 4 wt.% by ICP-MS.

In the contrast experiments, where the reductant NaH_2PO_2 was replaced with $NaBH_4$, larger sized Pt nanoparticles (NPs) loaded on $Ni(OH)_2$ NWs (Pt-NPs/$Ni(OH)_2$) were obtained. The TEM image of $Pt_{NP}/Ni(OH)_2$ in Fig. S8 illustrates that the $Ni(OH)_2$ NWs were homogeneously loaded with Pt NPs at an average size of ~3 nm. The EDS spectrum in Fig. S9 also proves the presence of platinum. The HRTEM image of the Pt NPs in inset of Fig. S8 confirms the inter-plane distance of the lattice fringe of 0.22 nm, which corresponds to that of the (111) facet of Pt. The ICP-MS measurement shows that the Pt content in $Pt_{NP}/Ni(OH)_2$ is about 4 wt.%.

The HER catalysis performance of the $Pt_c/Ni(OH)_2$ NWs was then evaluated in basic conditions using a traditional three electrode system. Fig. 3 shows the HER electrocatalytic activity of $Pt_c/Ni(OH)_2$ in H_2-saturated 0.1 mol L^{-1} KOH. The polarization curve of the $Pt_c/Ni(OH)_2$ in Fig. 3a demonstrates an onset overpotential of ~0 mV *vs.* RHE, and a significant low overpotential of 32 mV at a current density of 10 mA cm^{-2}, which is lower than that of the commercial 20% Pt/C (58 mV) and $Pt_{NP}/Ni(OH)_2$ (107 mV) at the same current density. In a sharp contrast, $Ni(OH)_2$ NWs alone exhibit rather poor HER activity under the similar condition, illustrating that the active sites of the $Pt_c/Ni(OH)_2$ for excellent HER performance are not provided by the $Ni(OH)_2$ NWs, but the Pt clusters. While, the $Ni(OH)_2$ NWs promote the dissociation of water and production of hydrogen intermediates and result in the unexceptionable HER activity of $Pt_c/Ni(OH)_2$ system in basic solutions [21–23]. The electrochemical active surface area (ECSA) of these electrocatalysts were estimated from the electrochemical double-layer capacitance (C_{dl}) in Fig. S10. As shown in Fig. S11, the C_{dl} of the $Pt_c/Ni(OH)_2$ NWs is 13.1 mF cm^{-2}, which is 1.47 times that of the $Pt_{NP}/Ni(OH)_2$ NWs (8.9 mF cm^{-2}). The enhanced ECSA of $Pt_c/Ni(OH)_2$ NWs can be attributed to the highly exposed and easily accessible active sites derived from the atomic-scale Pt clusters. In addition, if NaH_2PO_2 was not added in the

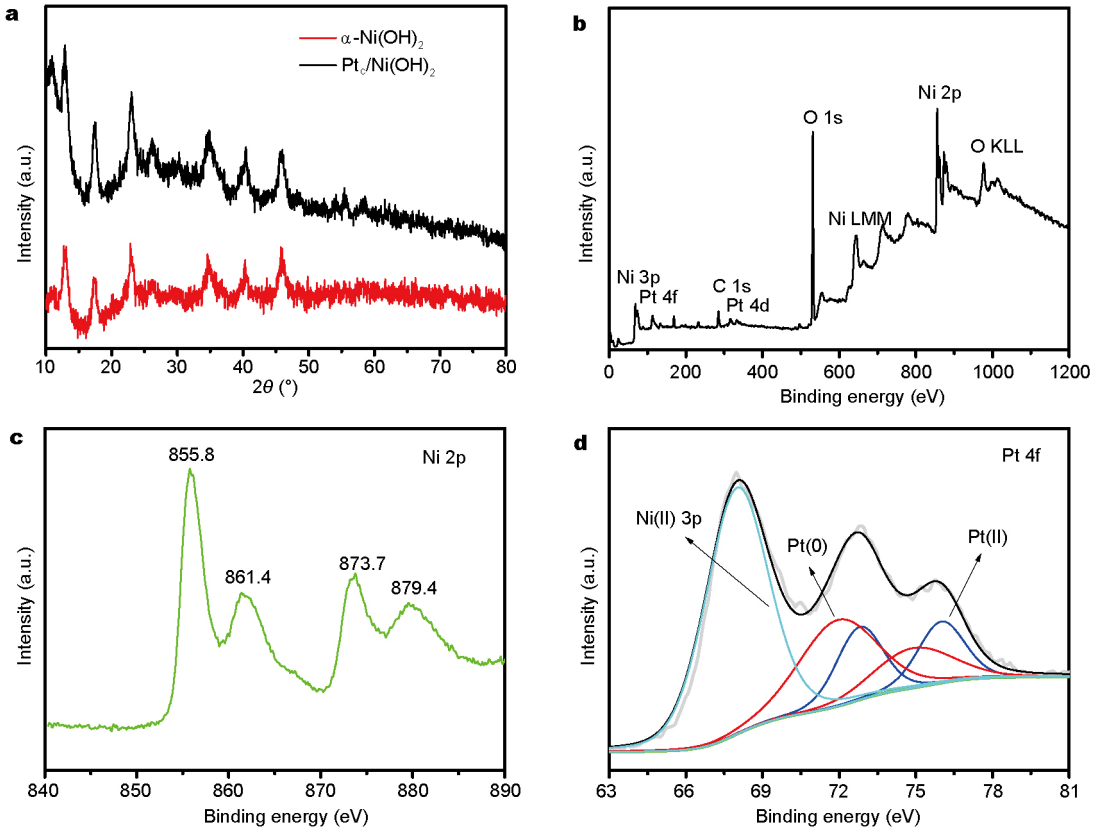

Figure 2 (a) Powder XRD spectra of α-$Ni(OH)_2$ and the as-prepared $Pt_c/Ni(OH)_2$. (b) XPS survey spectrum for $Pt_c/Ni(OH)_2$. (c) XPS spectra of high resolution Ni 2p regions and (d) Pt 4f regions.

synthesis process of $Pt_c/Ni(OH)_2$, a small amount of Pt(IV) would be adsorbed on the porous $Ni(OH)_2$ NWs ($Pt^{4+}/Ni(OH)_2$) by physical adsorption. The polarization curves in Fig. S12 illustrate that the $Pt^{4+}/Ni(OH)_2$ reveals poor HER performance in alkaline solution. All these data support the synergistic effects of Pt clusters and $Ni(OH)_2$ NWs in $Pt_c/Ni(OH)_2$ hybrid electrocatalyst for its exceptional HER activity. The HER performance of the $Pt_c/Ni(OH)_2$ NWs was further investigated in H_2-saturated 1 mol L^{-1} KOH using a traditional three electrode system. The polarization curves of the $Pt_c/Ni(OH)_2$ in Fig. S13 demonstrate a significant low overpotential of ~88 mV at a current density of 20 mA cm^{-2}, which is lower than that of the commercial 20% Pt/C (~107 mV) at the same current density.

The Tafel slope is an intrinsic property of the electrocatalyst that is determined by the rate-controlling step of the HER. For a whole HER process, the reaction steps involved to generate H_2 include Volmer reaction combined with Heyrovsky reaction or Tafel reaction, which is usually called Volmer-Heyrovsky or Volmer-Tafel mechanism. In alkaline condition, the Volmer reaction is the rate-controlling step of HER, due to the sluggish dissociation of water, giving rise to a Tafel slope of ~120 mV/dec for Pt/C. In Fig. 3b, the Tafel slope of $Pt_c/Ni(OH)_2$ is about 86 mV/dec, which is smaller than that of Pt/C (90 mV/dec). We speculated that this smaller Tafel slope of $Pt_c/Ni(OH)_2$ was not only attributed to the activity of atomic-scale Pt, but also ascribed to the $Ni(OH)_2$ substrate facilitating the decomposition of water. The mass activity of these electrocatalysts in Fig. 3c and Fig. S14 exhibits that $Pt_c/Ni(OH)_2$ reaches an extraordinarily high current density of ~6.34 A mg_{Pt}^{-1} at an overpotential of 50 mV in 0.1 mol L^{-1} KOH solution, which is approximately 28 and 6.8 times that of the commercial Pt/C (0.223 A mg_{Pt}^{-1}) and $Pt_{NP}/Ni(OH)_2$ (0.922 A mg_{Pt}^{-1}) at the same overpotential, respectively. The chronoamperometric curve in Fig. 3d reveals that the $Pt_c/Ni(OH)_2$ is stable with a constant current density of the complete HER process under a constant overpotential of 70 mV (*vs.* RHE). The typical serrate shape of the current density curve is attributed to the alternate bubble accumulation and bubble release on the electrocatalyst surface in the processes of hydrogen generation.

The performances of the $Pt_c/Ni(OH)_2$ NWs with different

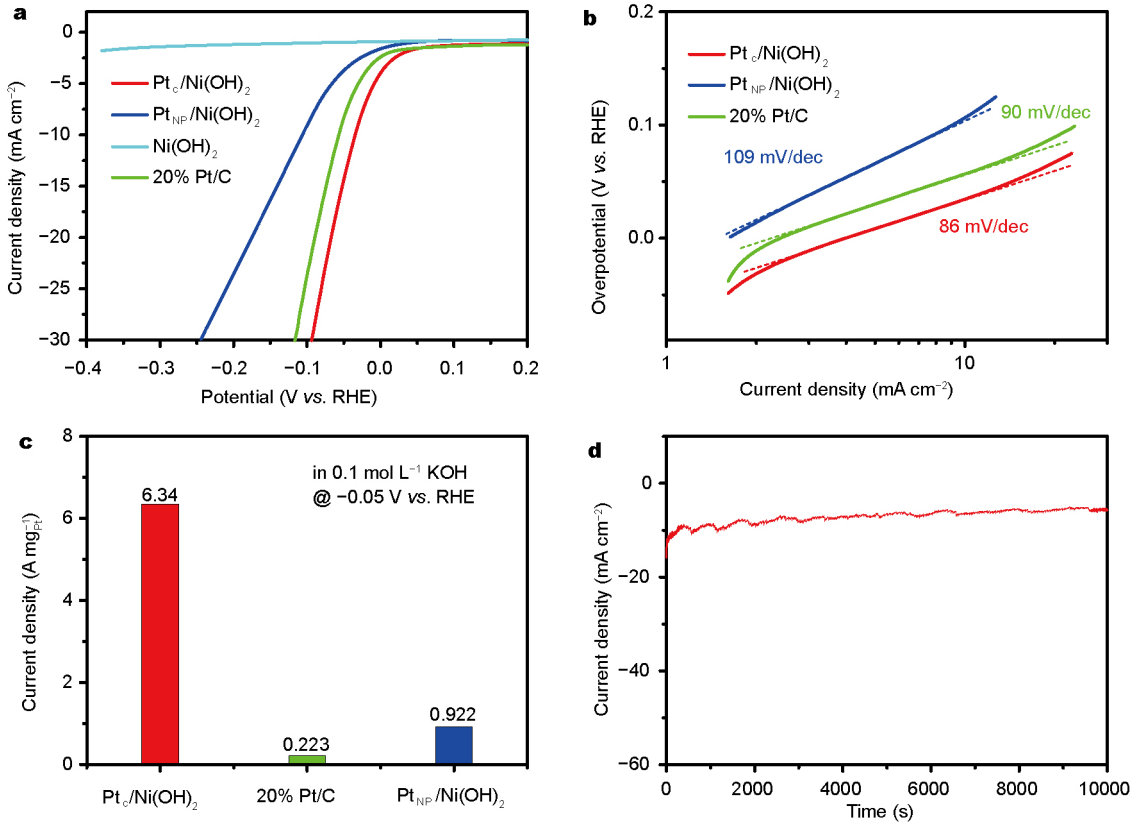

Figure 3 HER data of the catalysts in H_2-saturated 0.1 mol L^{-1} KOH. (a) Polarization curves of $Pt_c/Ni(OH)_2$, $Pt_{NP}/Ni(OH)_2$, commercial 20% Pt/C and $Ni(OH)_2$ NWs alone with a scan rate of 50 mV s^{-1}. (b) Tafel slopes of $Pt_c/Ni(OH)_2$, $Pt_{NP}/Ni(OH)_2$ and 20% Pt/C, respectively. (c) Mass current densities of $Pt_c/Ni(OH)_2$, $Pt_{NP}/Ni(OH)_2$ and 20% Pt/C at an overpotential of 0.05 V. (d) Chronoamperometric curve at a constant overpotential of 70 mV.

Pt mass loadings were further investigated. Fig. S15 show the TEM images and the EDS of $Pt/Ni(OH)_2$ with different Pt mass loadings. In the TEM image, there are no visible Pt NPs on the porous $Ni(OH)_2$ NWs, but the EDS reveals the presence of Pt. Subsequently, the HER performances of these materials in 0.1 mol L^{-1} KOH were measured. The HER data in Figs S16 and S17 illustrate that the Pt mass loading plays a crucial role in the HER performance of $Pt/Ni(OH)_2$.

In summary, we successfully synthesized a hybrid $Pt_c/Ni(OH)_2$ electrocatalyst, exhibiting extraordinary electrocatalytic performance for HER, which could be attributed to the following reasons: 1) the atomic-scale Pt clusters offer more active sites in comparison with Pt NPs at the same mass loading, vastly enhancing the catalytic performance and Pt atom utility. 2) The $Ni(OH)_2$ substrate promotes the dissociation of water and production of hydrogen intermediates, which subsequently adsorb on the catalyst and recombine into molecular hydrogen. 3) The α phase of $Ni(OH)_2$ NWs allows the anions to be loosely intercalated between the hydrated nickel hydroxide sheets, $[Ni(OH)_{2-x}(H_2O)_x]^{x+}$, thereby significantly promoting the dissociation of water in alkaline solutions.

CONCLUSIONS

In brief, we have successfully fabricated hybrid electrocatalyst of $Pt_c/Ni(OH)_2$ with atomic-scale Pt cluster decorated on porous α-$Ni(OH)_2$ NWs *via* a facile room-temperature synthesis strategy. Notably, the $Pt_c/Ni(OH)_2$ catalyst exhibits highly efficient HER performance under basic conditions. The $Pt_c/Ni(OH)_2$ shows an onset overpotential of ~0 mV *vs.* RHE, and a significantly low overpotential of 32 mV at a current density of 10 mA cm^{-2}, lower than that of the commercial 20% Pt/C (58 mV) at the same current density. The mass current density illustrated that the $Pt_c/Ni(OH)_2$ reached a high current density of 6.34 A mg^{-1}_{Pt} at an overpotential of 50 mV, which is approximately 28 times that of the commercial Pt/C (0.223 A mg^{-1}_{Pt}) at the same overpotential. The extraordinarily high activity of the hybrid catalyst is attributed to the atomic-scale Pt clusters offering more active sites, the $Ni(OH)_2$ substrate promoting the dissociation of water and production of hydrogen intermediates in

alkaline solutions. We expect that the rational design and facile synthetic strategy of the $Pt_c/Ni(OH)_2$ electrocatalyst could be extended to other catalysts for improved catalytic activity.

Received 12 March 2017; accepted 13 April 2017; published online 8 May 2017

1 Turner JA. Sustainable hydrogen production. Science, 2004, 305: 972–974
2 Yang H, Zhang Y, Hu F, *et al.* Urchin-like CoP nanocrystals as hydrogen evolution reaction and oxygen reduction reaction dual-electrocatalyst with superior stability. Nano Lett, 2015, 15: 7616–7620
3 Blakemore JD, Crabtree RH, Brudvig GW. Molecular catalysts for water oxidation. Chem Rev, 2015, 115: 12974–13005
4 Esswein AJ, McMurdo MJ, Ross PN, *et al.* Size-dependent activity of Co_3O_4 nanoparticle anodes for alkaline water electrolysis. J Phys Chem C, 2009, 113: 15068–15072
5 Jin H, Wang J, Su D, *et al. In situ* cobalt–cobalt oxide/N-doped carbon hybrids as superior bifunctional electrocatalysts for hydrogen and oxygen evolution. J Am Chem Soc, 2015, 137: 2688–2694
6 Luo J, Im JH, Mayer MT, *et al.* Water photolysis at 12.3% efficiency *via* perovskite photovoltaics and Earth-abundant catalysts. Science, 2014, 345: 1593–1596
7 Lu Q, Hutchings GS, Yu W, *et al.* Highly porous non-precious bimetallic electrocatalysts for efficient hydrogen evolution. Nat Commun, 2015, 6: 6567
8 McKone JR, Sadtler BF, Werlang CA, *et al.* Ni–Mo nanopowders for efficient electrochemical hydrogen evolution. ACS Catal, 2013, 3: 166–169
9 Raj IA, Vasu KI. Transition metal-based hydrogen electrodes in alkaline solution—electrocatalysis on nickel based binary alloy coatings. J Appl Electrochem, 1990, 20: 32–38
10 Crnkovic F. Electrochemical and morphological studies of electrodeposited Ni–Fe–Mo–Zn alloys tailored for water electrolysis. Int J Hydrogen Energ, 2004, 29: 249–254
11 Xu YF, Gao MR, Zheng YR, *et al.* Nickel/nickel(II) oxide nanoparticles anchored onto cobalt(IV) diselenide nanobelts for the electrochemical production of hydrogen. Angew Chem Int Ed, 2013, 52: 8546–8550
12 Gong M, Zhou W, Tsai MC, *et al.* Nanoscale nickel oxide/nickel heterostructures for active hydrogen evolution electrocatalysis. Nat Commun, 2014, 5: 4695
13 Fei H, Yang Y, Peng Z, *et al.* Cobalt nanoparticles embedded in nitrogen-doped carbon for the hydrogen evolution reaction. ACS Appl Mater Interfaces, 2015, 7: 8083–8087
14 Yan X, Tian L, He M, *et al.* Three-dimensional crystalline/amorphous Co/Co_3O_4 core/shell nanosheets as efficient electrocatalysts for the hydrogen evolution reaction. Nano Lett, 2015, 15: 6015–6021
15 Weng Z, Liu W, Yin LC, *et al.* Metal/oxide interface nanostructures generated by surface segregation for electrocatalysis. Nano Lett, 2015, 15: 7704–7710
16 Liu P, Zhao Y, Qin R, *et al.* Photochemical route for synthesizing atomically dispersed palladium catalysts. Science, 2016, 352: 797–800
17 Yang XF, Wang A, Qiao B, *et al.* Single-atom catalysts: a new frontier in heterogeneous catalysis. Acc Chem Res, 2013, 46: 1740–1748
18 Yan H, Cheng H, Yi H, *et al.* Single-atom Pd_1/graphene catalyst achieved by atomic layer deposition: remarkable performance in selective hydrogenation of 1,3-butadiene. J Am Chem Soc, 2015, 137: 10484–10487
19 Lin J, Wang A, Qiao B, *et al.* Remarkable performance of Ir_1/FeO_x single-atom catalyst in water gas shift reaction. J Am Chem Soc, 2013, 135: 15314–15317
20 Fei H, Dong J, Arellano-Jiménez MJ, *et al.* Atomic cobalt on nitrogen-doped graphene for hydrogen generation. Nat Commun, 2015, 6: 8668
21 Yin H, Zhao S, Zhao K, *et al.* Ultrathin platinum nanowires grown on single-layered nickel hydroxide with high hydrogen evolution activity. Nat Commun, 2015, 6: 6430
22 Subbaraman R, Tripkovic D, Strmcnik D, *et al.* Enhancing hydrogen evolution activity in water splitting by tailoring Li^+-$Ni(OH)_2$-Pt interfaces. Science, 2011, 334: 1256–1260
23 Subbaraman R, Tripkovic D, Chang KC, *et al.* Trends in activity for the water electrolyser reactions on 3d M(Ni,Co,Fe,Mn) hydr(oxy)oxide catalysts. Nat Mater, 2012, 11: 550–557
24 Gao M, Sheng W, Zhuang Z, *et al.* Efficient water oxidation using nanostructured α-nickel-hydroxide as an electrocatalyst. J Am Chem Soc, 2014, 136: 7077–7084
25 Rajamathi M, Vishnu Kamath P. On the relationship between α-nickel hydroxide and the basic salts of nickel. J Power Sources, 1998, 70: 118–121
26 Dong X, Guo Z, Song Y, *et al.* Flexible and wire-shaped micro-supercapacitor based on $Ni(OH)_2$-nanowire and ordered mesoporous carbon electrodes. Adv Funct Mater, 2014, 24: 3405–3412

Acknowledgments The authors thank the financial support from the National Natural Science Foundation of China (21425103, 21673280 and 11374039).

Author contributions Wang Q designed and engineered the experiments; Yang H performed the experiments, analyzed the data and wrote the paper with support from Wang C, Hu F, Zhang Y and Lu H. All authors contributed to the general discussion.

Conflict of interest The authors declare that they have no conflict of interest.

Supplementary information Supporting data are available in the online version of the paper.

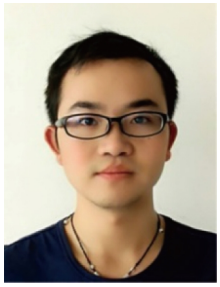

Hongchao Yang is now a PhD candidate from Suzhou Institute of Nano-Tech and Nano-Bionics, Chinese academy of sciences. His current research is focused on the electrocatalysis for hydrogen evolution and oxygen reduction reaction.

Qiangbin Wang is the Director for the Key Laboratory of Nano-Bio Interface, Chinese Academy of Sciences and Professor of Physical Chemistry at Suzhou Institute of Nano-tech Nano-bionics, Chinese Academy of Sciences. His research interest mainly concentrates on the controlled synthesis and self-assembly of inorganic nanocrystals and their applications in optoelectronics, catalysis and biomedicine.

原子级Pt团簇修饰的α相氢氧化镍纳米线作为高效析氢反应催化剂

杨红超[1,2], 汪昌红[1,2], 胡峰[2], 张叶俊[2], 卢欢[2], 王强斌[1,2,3*]

摘要 合成原子级别的催化剂是一项颇具前景但又充满挑战的课题. 本文通过简单的室温反应成功制备了一种原子级别的Pt团簇修饰的多孔α相氢氧化镍纳米线($Pt_c/Ni(OH)_2$)复合材料. 所得到的$Pt_c/Ni(OH)_2$在碱性环境下表现出高效的电催化析氢反应性能. 在氢气饱和的0.1 mol L^{-1}氢氧化钾溶液中, $Pt_c/Ni(OH)_2$的起始过电势很小, 接近于0, 当电流密度为10 mA cm^{-2}时, 其过电势低至32 mV. 此过电位低于同等条件下商业化20% Pt/C的过电势(58 mV). 通过质量电流密度数据显示, 在过电势为50 mV时, $Pt_c/Ni(OH)_2$的质量电流密度高达6.34 A mg_{Pt}^{-1}, 在同样的过电势条件下, 这一电流是商业化Pt/C (0.223 A mg_{Pt}^{-1})的28倍, 表明我们所制得的$Pt_c/Ni(OH)_2$在碱性环境下具有高效的电催化析氢反应性能.